Vol. 283: 55–71, 2004 | MARINE ECOLOGY PROGRESS SERIES
Mar Ecol Prog Ser | Published November 30

Characteristics of the chemical plume behind a sinking particle in a turbulent water column

André W. Visser[1,*], George A. Jackson[2]

[1]Danish Institute for Fisheries Research, Kavalergården 6, 2920 Charlottenlund, Denmark
[2]Department of Oceanography, Texas A&M University, College Station, Texas 77843, USA

ABSTRACT: Many aquatic organisms, from bacteria to crustaceans, use chemical plumes released by sinking particulate organic material either directly as a food source or as a signal to find potential food items (marine snow aggregates, fecal pellets). This work examines how the relevant metrics of the plume (length, volume and cross sectional area) relate to encounter rates and how they vary with turbulence. Total plume length appears to be invariant to turbulent shear rate, although plume volume and cross section do decrease strongly with increased turbulence. Turbulence can also break a plume into multiple segments. The length of the segment connected to the particle (the first unbroken segment) tends to be about 50% of the total plume length, as well as containing about half of the total plume volume and cross sectional area. Despite the complexity of the processes involved, these relationships can be described by relatively simple functions that are revealed both empirically through modelling and through theoretical analysis. The critical parameter is γT_0^*, the product of the average turbulent shear rate and the diffusive time scale — the length of time a plume would last in calm water. The results highlight the ecological differences associated with different turbulence intensities as a function of depth in the water column.

KEY WORDS: Turbulence · Marine snow · Fecal pellet · Dissolved organic matter · Chemical trail · Encounter rate

INTRODUCTION

Although seemingly uniform, the aquatic environment in which plankton live is filled with ephemeral chemical and physical cues that have scales of meters and smaller. Chemical plumes trail behind falling particles and swimming animals; small velocity perturbations follow swimming or feeding copepods. The ability of an organism to survive depends on its use of these signals to find food and mates, and to avoid predation; understanding of the planktonic ecosystem depends on our ability to understand and describe the heterogeneity of this world. Previous work to fill in the details of this world has focussed on velocity and pressure perturbations induced by swimming and feeding zooplankton (Yen & Strickler 1996, Kiørboe & Visser 1999, Visser 2001, Jiang et al. 2002), and the chemical plumes associated with leaking phytoplankton (e.g. Jackson 1989, Bowen et al. 1993) and falling marine snow particles (Kiørboe et al. 2001, Kiørboe & Thygesen 2001) in the absence of background water motions. To understand natural aquatic systems, we need to be able to describe how these signals are modified by turbulent water movement.

The physics relevant to particulate organic matter includes the control of particle settling and associated water movement, and the subsequent diffusive spread of released molecules. Organic matter released by falling particles can provide localized food resources for microbes in the surrounding water column and provide chemical cues for animals and microbes to locate the particles. Copepods, for instance, respond to dissolved organic material in the water and can follow a chemical trail to a sinking aggregate or to other animals (Poulet & Ouellet 1982, Kiørboe 2001). The detection of a specific particle depends on the rate at which

*Email: awv@dfu.min.dk

the particle releases material, its sinking rate, the chemical nature and the molecular diffusivity of the chemical substrate, and the minimum concentration (threshold) detectable by an organism. The detection threshold allows us to define boundaries for the chemical plume that can be species-specific. By using a threshold concentration for detections, we can place boundaries on the chemical plumes and determine their geometric properties for different conditions.

Plumes offer significantly different resources for osmotrophs and for hunters. For understanding bacteria or phytoplankton located in the enriched environment behind a leaky detrital particle or zooplankter, the plume volume defines the favourable region. Used in conjunction with information on particle or animal distributions, it can be used to describe the heterogeneity of the chemical environment (Jackson & Kiørboe 2004). For understanding zooplankton search behaviour, plume length and cross-sectional area have been used to describe the rate of finding particulate targets (Jackson & Kiørboe 2004). For example, the detectable plume behind a large falling particle in still water could be as long as 1 m (Kiørboe & Thygesen 2001). This estimate of plume length does not account for the effects of turbulence in lengthening or in disrupting the plume. While relevant plume properties can be estimated using analytic solutions in still water (Jackson & Kiørboe 2004), the techniques provide no insight into the effect of natural turbulence on plume structure.

Turbulence is an inherent property of fluid flows that is important to planktonic organisms because of effects ranging from increasing the rate of nutrient uptake by phytoplankton (Munk & Riley 1952, Gavis 1976, Lazier & Mann 1989, Karp-Boss et al. 1996) to increasing the rate of encounter between zooplankton predators and their prey (Rothschild & Osborn 1988). Turbulence also accelerates the coagulation processes, which form large marine snow particles and the disaggregation processes that shrink them (e.g. Jackson & Burd 1998).

Turbulence can change the structure of the chemical plume strung out behind a falling particle. The straining of water containing a plume stretches it out, increasing its length, at the same time increasing diffusion gradients, causing enhanced diffusive transport and decreased plume lifetime. Thus, turbulence could enhance the plume length or decrease the plume volume. Because the rate of stretching is not uniform along the length of the plume, it could also disrupt the plume by forming one or more breaks along its length where local concentrations fall below the detection ability of searching organisms. For chemosensory animals searching for a particle or a mate, important plume properties include the length and cross-section of the unbroken plume segment, the sizes of gaps along the plume and whether the animals can span these gaps in a successful search for the particle; for free living bacteria or phytoplankton feeding on the enriched chemical environment, important properties include the plume volume, its patchiness and the time scale over which patches exist. Since many of the important particle properties depend on size, the particle size distribution is an important property for relating interactions between particles and organisms to their ecological impact.

The ecological role of turbulence is enhanced by its spatial and temporal variability. Because turbulence is a means of dissipating hydrodynamic energy as heat, the highest turbulence rates are associated with energetic regions, such as near the wind-blown ocean surface. Sub-thermocline depths have fewer energy sources and much weaker turbulent motions. As a result, the effect of turbulence on the heterogeneity of dissolved organic matter distributions as well as the detection, colonization and grazing of particulate matter should vary between the surface mixed layer, the thermocline and the mesopelagic realm.

In this article, we develop a simplified model describing the effect of turbulence on the chemical plume trailing behind any moving particle or animal, although we focus on falling particles. We use the model to explore where and how extensively turbulence affects the ability of zooplankton to detect falling particles. We also explore how turbulence conditions affect the micro-patchiness of the marine environment by comparing plume properties for different particle types under different energy dissipation rates. In Table 1, we provide a list of parameters, notation and typical values used in this work.

THE MODEL

The non-turbulent case

Particle size-dependence. The settling rates of marine snow (Alldredge & Gotschalk 1988, Alldredge & Gotschalk 1989) and fecal pellets (Small et al. 1979) have been described using a power law dependence on particle size. Similar power law relationships exist for the organic content of particulate matter (Alldredge 1998), and for the rate at which amino acids and other dissolved organic compounds are released (Kiørboe & Thygesen 2001). While there is considerable variability in observations, these relationships provide an initial means of characterizing the importance of particle size. In this, we follow the formulations suggested by Jackson & Kiørboe (2004) for modelling the settling rate w and leakage rate L for particles of size r.

Detection threshold. The concentration at which an organism can detect the plume, C^*, is crucial for deter-

Table 1. Notation and typical parameter values

Symbol	Description	Value	Units
$\mathbf{a}_n$, $\mathbf{b}_n$	Fourier coefficients. Direction chosen randomly in 3D		cm s^{-1}
C	Concentration at centre of radial solute distribution		mol cm^{-3}
C^*	Minimum detectable solute concentration	10^{-12} to 10^{-10}	mol cm^{-3}
D	Molecular diffusivity	10^{-5}	cm^2 s^{-1}
I	Integral length scale	50 to 1000	cm
i,j	As subscripts on λ, ϕ, ℓ, C etc implies evaluation for segment j at time $i\delta$		
k_n	Wave number of n^{th} Fourier mode; $k_n = \|\mathbf{k}_n\|$		cm^{-1}
$\mathbf{k}_n$	Wave vector of n^{th} Fourier mode. Direction chosen randomly in 3D		cm^{-1}
L	Leakage rate	10^{-10} to 10^{-16}	mol s^{-1}
ℓ	Length of a plume segment		cm
r	Particle radius	0.002 to 0.5	cm
s	Straining ratio over a small time step		
T^*	Diffusive time scale: time for which segment remains detectable; T_0^* for no turbulence		s
$\mathbf{u}$	Turbulent velocity field (3D)		cm s^{-1}
U	RMS turbulent velocity		cm s^{-1}
V^*	Volume of plume above concentration threshold; V_0^* for no turbulence, V_1^* for 1st unbroken segment		cm^3
w	Particle settling speed	0.01 to 1	cm s^{-1}
$\mathbf{x}^\bullet$	Trajectory of sinking particle (3D)		cm
$\mathbf{x}^*$	Trajectory of a plume tracer (3D)		cm
x_1^*	Straight line (Euclidean) distance of first gap in plume		cm
X_1^*	Straight line (Euclidean) length of first plume segment		cm
Z^*	Length of plume above concentration threshold; Z_0^* for no turbulence, Z_1^* for 1st unbroken segment.		cm
δ	A small time step		s^{-1}
ε	Energy dissipation rate	1 to 10^{-10}	cm^2 s^{-3}
ϕ	Solute concentration		mol cm^{-3}
γ	Turbulent rate of strain (material line): $\gamma = (\varepsilon/6\nu)^{1/2}$	10^{-4} to 10	s^{-1}
η	Kolmogorov length scale: $\eta = (\nu^3/\varepsilon)^{1/4}$	0.03 to 10	cm
λ	Radial length scale of solute distribution		cm
λ_B	Batchelor scale: $\lambda_B = (\nu D^2/\varepsilon)^{1/4}$		
λ_T	Taylor microscale: $\lambda_T = (15\nu U^2/\varepsilon)^{1/2}$	1 to 100	cm
ν	Molecular viscosity	10^{-2}	cm^2 s^{-1}
ν_T	Turbulent viscosity		cm^2 s^{-1}
ρ	Radial coordinate in cylindrical coordinates		cm
ρ^*	Width of plume; ρ_0^* for no turbulence		cm
σ^*	Cross sectional area of plume above concentration threshold; σ_0^* for no turbulence, σ_1^* for 1st unbroken segment		cm^2
ω_n	Frequency of n^{th} mode		s^{-1}
ξ	Length of a material line		cm

mining the extent of a plume. Its value is clearly specific to organism and compound. Using observed background concentrations (e.g. Poulet et al. 1991, Suttle et al. 1991), and observed responses by copepod (Yen et al. 1998) and bacteria (Carlucci et al. 1986, Atema 1988, Suttle et al. 1991), Kiørboe & Thygesen 2001) estimated a value of 4×10^{-11} mol cm^{-3} (40 nM), while Jackson & Kiørboe 2004) used a value of 3×10^{-11} mol cm^{-3} (30 nM).

Plume properties. Kiørboe et al. (2001) presented a numerical solution for the concentration field around a falling sphere for Reynolds number ≤10, which incorporated molecular diffusion of the substrate and laminar flow around the particle. Jackson & Kiørboe (2004) showed that analytical solutions describing the concentrations of substrate leaked from a moving point source and then diffused away provide the same estimates for the plume length and width as the numerical solutions at low Re, and could provide the same answers with suitable corrections for higher Re. Their uncorrected plume length is:

$$Z_0^* = \frac{L}{4\pi D C^*} \quad (1)$$

where C^* is the threshold detection concentration, D is the molecular diffusivity and L the leakage rate of material from the particle as it sinks with velocity w. Similarly, the plume width is:

$$\rho_0^* = \left(\frac{4Dz}{w}\ln\frac{L}{4\pi DC^* z}\right)^{0.5} \quad (2)$$

where z is the distance from the sinking particle along the plume. The plume cross-section (i.e. the plume's projection onto a vertical plane) is given by:

$$\sigma_0^* = \frac{0.24}{Dw^{0.5}}\left(\frac{L}{\pi C^*}\right)^{1.5} \quad (3)$$

and the plume volume is:

$$V_0^* = \frac{D}{w}\pi Z_0^{*2} \quad (4)$$

An additional measure of the plume for non-turbulent situations is:

$$T_0^* = \frac{Z_0^*}{w} = \frac{L}{4\pi DwC^*} \quad (5)$$

which is the time after release it takes for the concentration in a small section of the plume to fall below the detection threshold.

Effect of turbulence

Describing turbulence. Turbulent intensity in the marine environment varies greatly in time and space. The most common description of turbulence is the energy dissipation rate ε; with measured values ranging from 10^{-6} to 1 cm^2 s^{-3}. Higher values are typically found in the surface mixed layer under strong wind conditions and in strong flows over tidally-dominated shallow shelf seas; lower values are found in the pycnocline and in the deeper mesopelagic region (e.g. Gargett 1997, Visser et al. 2001, Yamazaki et al. 2002). In Kolmogorov's theory of fully developed 3D isotropic turbulence, the inertial sub-range of the turbulent energy spectrum is fully specified by 3 parameters: ε, the kinematic viscosity ν and the integral length scale I. The latter is a measure of the size of the energy-containing eddies and has values ranging from several meters in the surface mixed layer to several centimetres in the pycnocline (e.g. Yamazaki et al. 2002, Maar et al. 2003). These 3 parameters can be related to others also used to describe turbulent systems, including the root mean square turbulent velocity $U = (\varepsilon I)^{1/3}$, turbulent eddy viscosity $\nu_T = (I^4\varepsilon)^{1/3}$, the Taylor microscale $\lambda_T = (15\nu U^2/\varepsilon)^{1/2}$ (the characteristic length scale of turbulent velocity gradients) and the microstructure rate of strain $\gamma_T = (\varepsilon/2\nu)^{1/2}$.

Kinematic simulations. Turbulence-like flow fields can be simulated by superimposing a number of random Fourier velocity modes chosen to conform to given physical constraints (Kraichnan 1970, Fung et al. 1992). While such flow fields are not fully consistent with fully developed isotropic turbulence (Yamazaki et al. 2004, see 'Discussion), they share many relevant characteristics (Malik & Vassilicos 1999). The simulated field is constructed such that its kinetic energy spectrum reflects the turbulent energy spectrum (e.g. the classic $k^{-5/3}$ energy cascade of Kolmogorov) and that its flow field is non-divergent. Simulations are specified through the 3 parameters mentioned earlier: ε, ν and I. Fluid elements or parcels can be tracked by integrating the velocity field. To date, such models have been used primarily to investigate physical phenomena (Fung 1993, Fung 1998). More recently, biological aspects have been incorporated into this method, for instance, in re-examining the Rothschild-Osborn turbulent encounter process (Lewis & Pedley 2000, Lewis & Pedley 2001).

The Fourier method. The energy spectrum $E(k)$ describes distribution of kinetic energy in terms of wave number k. In the Fourier approach, the spectrum is divided into N bands, where the width and representative wave number of the n^{th} band are δk_n and k_n. The turbulent velocity vector field $\mathbf{u}(\mathbf{x},t)$ at any location $\mathbf{x}$ and time t is described as the sum of Fourier components (e.g. Lewis & Pedley 2000):

$$\mathbf{u}(\mathbf{x},t) = \sum_{n=1}^{N}\left[\left(\mathbf{a}_n\times\hat{\mathbf{k}}_n\right)\cos\left(\mathbf{k}_n\cdot\mathbf{x}+\omega_n t\right)\right] + \sum_{n=1}^{N}\left[\left(\mathbf{b}_n\times\hat{\mathbf{k}}_n\right)\sin\left(\mathbf{k}_n\cdot\mathbf{x}+\omega_n t\right)\right] \quad (6)$$

where $\hat{\mathbf{k}}_n = \mathbf{k}_n/k_n$ is the unit vector defining the direction of the n^{th} wave vector $\mathbf{k}_n$, $k_n = |\mathbf{k}_n|$, ω_n is its angular frequency, $\mathbf{a}_n$ and $\mathbf{b}_n$ are the associated amplitude vectors, and the cross term ensures that the flow field is non-divergent. The amplitudes of $\hat{\mathbf{k}}_n$, $\mathbf{a}_n$ and $\mathbf{b}_n$ are calculated as given below, but their directions are chosen to be random in 3 dimensions.

We use a simple Kolmogorov energy spectrum:

$$E(k) = E_0 k^{-5/3} \quad (7)$$

although other spectral shapes can also be used (Fung & Vassilicos 1998, Malik & Vassilicos 1999, Lewis & Pedley 2001). N discrete wave numbers are chosen to lie between $k_1 = I^{-1}$ and $k_N = \eta^{-1}$ where $\eta = (\nu^3/\varepsilon)^{1/4}$ is the Kolmogorov length scale, and is a measure of the scale ($2\pi\eta$) at which viscous dissipation of energy becomes important (Gargett 1997). The energy spectrum has cut-offs at k_1 and k_N: $E(k) = 0$ for $k < k_1$ and $k > k_N$. To avoid harmonic effects, discrete wave numbers are distributed in a geometric series from k_1 to k_N:

$$k_n = \frac{1}{\eta}\left(\frac{\eta}{I}\right)^{\frac{n-1}{N-1}} \quad (8)$$

The values of $\delta k_n = (k_{n+1} - k_{n-1})/2$ for $n = 2, \ldots, N-1$, $\delta k_1 = (k_2 - k_1)/2$ and $\delta k_N = (k_N - k_{N-1})/2$. The frequency of the n^{th} mode is:

$$\omega_n = 0.4\sqrt{k_n^3\, E(k_n)} \quad (9)$$

where the factor 0.4 (the unsteadiness parameter) is set in accordance with Malik & Vassilicos (1999). The coefficient $E_0 = 1.5\varepsilon^{2/3}[1 - (\eta/I)^{4/3}]^{-1}$, so that the appropriate condition relating ε and $E(k)$ are met (Tennekes & Lumley 1972). The amplitudes of $\mathbf{a}_n$ and $\mathbf{b}_n$ are given by:

$$|\mathbf{a}_n|^2 = |\mathbf{b}_n|^2 = 2E(k_n)\delta k_n \tag{10}$$

Plume construction. We calculate the trajectory of a particle $\mathbf{x}^\bullet(t)$ by integrating the velocity along its path:

$$\frac{d\mathbf{x}^\bullet}{dt} = \mathbf{u}(\mathbf{x}^\bullet,t) + w\hat{\mathbf{z}}, \qquad \text{for } t \in [0,T] \tag{11}$$

for a given initial position $\mathbf{x}^\bullet_0$, using the turbulent flow field $\mathbf{u}$ given in the previous section and sinking velocity $w\hat{\mathbf{z}}$ (cf. Fig. 1).

We release neutrally buoyant parcels into the flow field at discrete time intervals along the particle's trajectory. If the aggregate is at $\mathbf{x}_i = \mathbf{x}^\bullet(t_i)$ at time t_i, then the path of the i^{th} parcel is:

$$\frac{d\mathbf{x}_i^*}{dt} = \mathbf{u}(\mathbf{x}_i^*,t), \quad \text{for } t \in [t_i,T] \text{ and } \mathbf{x}_i^*(t=t_i) = \mathbf{x}^\bullet(t_i) \tag{12}$$

The time series $\mathbf{x}^*_j(t)$ for $t \in [t_i,T]$ is the path of an idealized tracer marking out a location in the centre of the plume. In comparison, at any given time t_i, the series of points $\mathbf{x}^*_j(t_i)$ for $j = 1 \ldots i$, defines the material line along the centre of the plume. The separation between 2 successive points along the material line is:

$$\ell_{i,j} = |\mathbf{x}^*_j(t_i) - \mathbf{x}^*_{j+1}(t_i)| \tag{13}$$

providing a measure of the stretching (or squashing) of the plume centreline by turbulent straining.

Diffusion and concentration. We treat each plume section as a small cylinder of solute having length $\ell_{i,j}$ that is spread both perpendicular to the axis by diffusion and along the axis by turbulence. In order to make this problem tractable, we assume that the diffusion and stretching can be treated separately within a short time step δ. We assume an initial Gaussian distribution of solute around the central axis of each cylinder:

$$\phi_{i,j} = C_{i,j}e^{-\rho^2/\lambda_{i,j}^2} \tag{14}$$

where $C_{i,j}$ is the concentration along the central axis, ρ is the distance from the central axis, $\lambda_{i,j}$ is a measure of the radial distribution of solute for the j^{th} line element at time since release of $t = i\delta$. The combined action of both turbulent straining and diffusion over the short time step δ gives the resultant solute distribution:

$$\begin{aligned}\phi_{i+1,j} &= \frac{C_{i,j}\lambda_{i,j}^2 s_{i,j}}{4D\delta + \lambda_{i,j}^2 s_{i,j}} \exp\left(-\frac{\rho^2}{4D\delta + \lambda_{i,j}^2 s_{i,j}}\right) \\ &= C_{i+1,j}\exp\left(-\frac{\rho^2}{\lambda_{i+1,j}^2}\right)\end{aligned} \tag{15}$$

where $s_{i,j} = \ell_{i,j}/\ell_{i+1,j}$ measures stretching of the line segment by straining and D is the molecular diffusivity (see Appendix 1 for details). Both straining and diffusion transform one Gaussian distribution into another, suggesting that the time evolution of the solute distribution is fully prescribed for both processes by the recursion formulae:

$$\lambda_{i+1,j}^2 = 4D\delta + \lambda_{i,j}^2 \frac{\ell_{i,j}}{\ell_{i+1,j}} \tag{16}$$

$$C_{i+1,j} = C_{i,j}\frac{\lambda_{i,j}^2}{\lambda_{i+1,j}^2}\frac{\ell_{i,j}}{\ell_{i+1,j}} \tag{17}$$

which are closed with the initial conditions:

$$\lambda_{1,j}^2 = 4D\delta \tag{18}$$

$$C_{1,j} = \frac{L}{4\pi D w \delta} \tag{19}$$

These relationships are developed in Appendix 1. If the threshold concentration for detection is C^*, then the detection distance from the central axis of the cylinder $\rho_{i,j}^*$ is:

$$\rho_{i,j}^* = \lambda_{i,j}\left(\ln\left(\frac{C_{i,j}}{C^*}\right)\right)^{1/2} \tag{20}$$

from which the cross section and volume of the plume can be calculated. The width of the plume reduces to 0 if $C_{i,j}$ is less than the threshold concentration, but the position of the plume centreline given by $\mathbf{x}_i^*$ is valid for all times and concentrations.

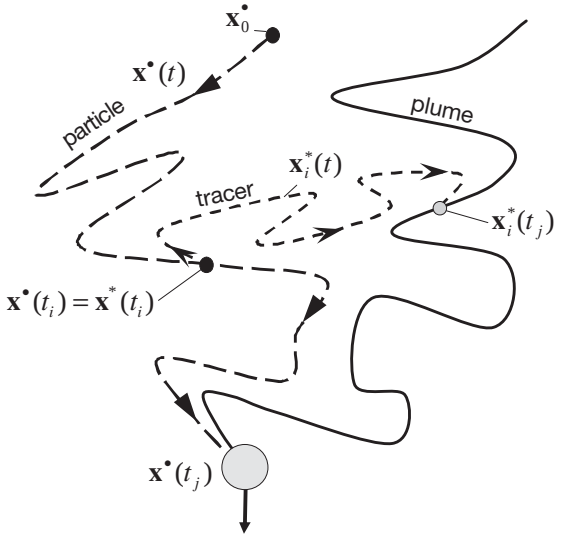

Fig. 1. The plume construct: $\mathbf{x}^\bullet(t)$, the trajectory of a sinking particle released from an initial location $\mathbf{x}^\bullet_0$, under the influence of uniform sinking rate and turbulence. $\mathbf{x}^*_i(t)$, the trajectory of a neutrally buoyant particle released from $\mathbf{x}^\bullet(t_i)$, a point along the particle path. The locus of points $\mathbf{x}^*_i(t_j)\ \forall\ i$, defines the plume position at time t_j

Table 2. The detection time scale T_0* and detection length scale Z_0* under still conditions computed for the marine snow and fecal pellet size dependent (r, equivalent particle radius) relationships to sinking speed w and leakage rate L and for specific detection thresholds C*

				C* mol cm^{-3}					
				2×10^{-12}		1×10^{-11}		5×10^{-11}	
	r (cm)	w (cm s^{-1})	L (mol s^{-1})	T_0* (s)	Z_0* (cm)	T_0* (s)	Z_0* (cm)	T_0* (s)	Z_0* (cm)
Marine snow	0.02	0.047	2.8×10^{-15}	240	11	48	2.3	10	0.45
	0.1	0.071	3.2×10^{-14}	1800	130	350	25	280	5.0
	0.5	0.11	3.5×10^{-13}	13000	1400	1300	280	520	56
Fecal pellet	0.002	0.011	9.7×10^{-17}	36	0.38	7.2	0.077	1.4	0.015
	0.008	0.17	6.2×10^{-15}	145	25	29	4.9	5.8	1.0
	0.02	1.1	9.7×10^{-14}	360	380	72	77	14	15

Calculations. The model was run for 4 different levels of turbulence ranging from 10^{-6} to 1 cm^2 s^{-3}, for 3 different particle sizes, and for marine snow and fecal pellet parameterisations of sinking and leakage rates (Table 2). For each particle size-type-turbulence combination, there were 4 replicate runs. The integral length scale was set to 100 cm in most cases, a value representative of the surface and thermocline conditions (Yamazaki et al. 2002). The turbulence velocity field was simulated using $N = 41$ Fourier modes. Time steps δ varied between simulations to ensure that the distance between particles remained less than the Kolmogorov scale for the times up to the non-turbulent time scale (Eq. 5); δ varied from 0.001 s for fast sinking particles in high turbulence to 10 s for slow sinking particles in low turbulence.

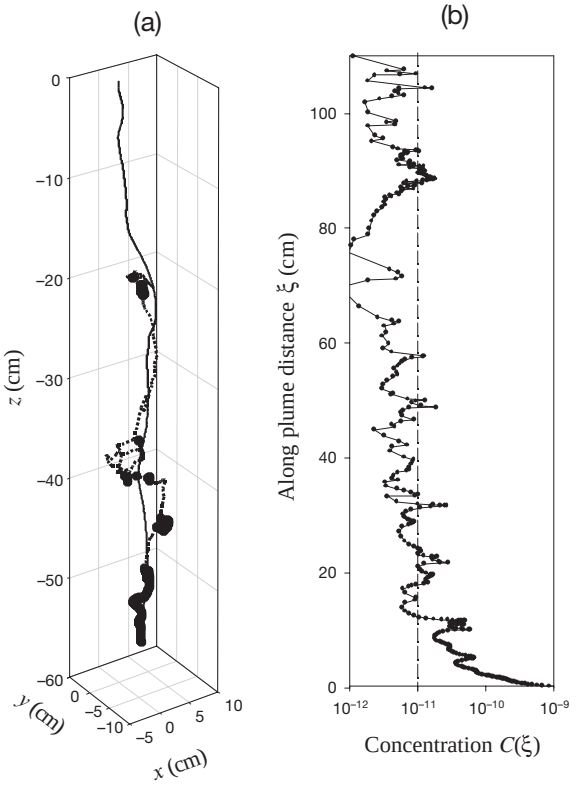

Fig. 2. Example of spatial structure of a particle trajectory and its plume. (a) Black line: trajectory of a sinking marine snow particle ($r = 0.1$ cm, $w = 0.07$ cm s^{-1}, $L = 3 \times 10^{-14}$ mol s^{-1}) under turbulent conditions ($\varepsilon = 10^{-4}$ cm^2 s^{-3}, $I = 100$ cm); dotted line: the central location of the plume trailing behind it at time t = 950 s. Points exceeding a detection threshold (C* = 10^{-11} mol cm^{-3}) are marked with plotting symbols. (b) The concentration of exudates released by the particle along the central (material line) of the plume. For this case, the non-turbulent length and time scales are Z_0* = 25 cm and T_0* = 350 s, respectively

Each of these simulations was analysed using 3 different detection threshold concentrations (Table 2), corresponding to a possible range for both bacteria and copepods. For each detection threshold, the detectable length (Z), cross sectional area (σ) and volume (V) of the plume were calculated for slightly different definitions of plume length: the total detectable plume (Z*, σ*, V*) and the unbroken plume next to the sinking particle (Z_1*, σ_1*, V_1*).

In order to highlight how the various plume metrics vary with turbulence, we express the variation of turbulence in terms of the parameter γT_0*, the product of the non-turbulent plume diffusive time scale and the average turbulent rate of strain associated with material line deformation, $\gamma = (\varepsilon/6\nu)^{1/2}$.

Calculations were performed using code written in MATLAB, with a 4th order Runge-Kutta solution scheme used to integrate particle trajectories.

RESULTS

A typical simulation result shows a clear primary plume (~12 cm), as well as numerous patches with detectable concentrations scattered along the plume's length out to a considerable distance, as in a patch

about 3 cm long that is 90 cm down the plume (Fig. 2a,b). The concentration distribution along plume reflects the processes responsible (Fig. 2b). The low concentrations between 60 and 80 cm are associated with a large degree of stretching experienced by that section of the plume, as can be deduced from the relatively wide spacing between points in the region. In comparison, the high concentrations at 90 cm are associated with low stretching (a high density of points). Thus, the along-plume variation of solute concentration is associated with the variation in cumulative along-plume stretching.

At the start of a simulation, the unbroken and total plume lengths are the same (Fig. 3). This is the period of plume development. Measures of the total and unbroken plume diverge thereafter, although both sets vary. To avoid initialisation artefacts, we analysed only those data for the periods after the time of the first break or the time scale for a non-turbulent plume T_0*, whichever comes first.

Total plume metrics

Simulation results. The normalized total volume of the plume V^*/V_0^* shows a consistent trend for both marine snow (Fig. 4a) and fecal pellets (Fig. 4b), with $V^*/V_0^* \approx 1$ for $\gamma T_0^* \ll 1$ and $V^*/V_0^* \approx 0$ for $\gamma T_0^* \gg 1$. Similar trends are exhibited by the normalized total cross section of the plume σ^*/σ_0^* (Fig. 4c,d). The volume and cross section can be reasonably well modelled by empirical functions of the form:

$$f^* = \frac{f_0^*}{1 + a\gamma T_0^*} \quad (21)$$

(Table 3). In all cases, the fit is highly significant ($p < 0.0001$).

In contrast, there is no similar trend in the normalised total plume length (Fig. 4d,e). The total plume length Z^* is approximately equal to Z_0^* for all levels of turbulence, although the variance does increase for $\gamma T_0^* \gg 1$.

Theoretical justification. A simplistic theoretical argument explains these results. Under uniform straining γ, the distance along a material line laid out by a sinking particle is $\xi(t) = (e^{\gamma t} - 1)w/\gamma$ (Eq. A2-4; Appendix 2). Under the same conditions, the concentration at the central axis is $C(t) = L/(4\pi D\xi(t))w/\gamma$ (Eq. A1-15). Thus, the time at which a plume segment becomes undetectable is given by:

$$T^* = \frac{1}{\gamma}\ln(\gamma T_0^* + 1) \quad (22)$$

and the length of the plume by:

$$Z^* = \xi(T^*) = \frac{L}{4\pi D C^*} = Z_0^* \quad (23)$$

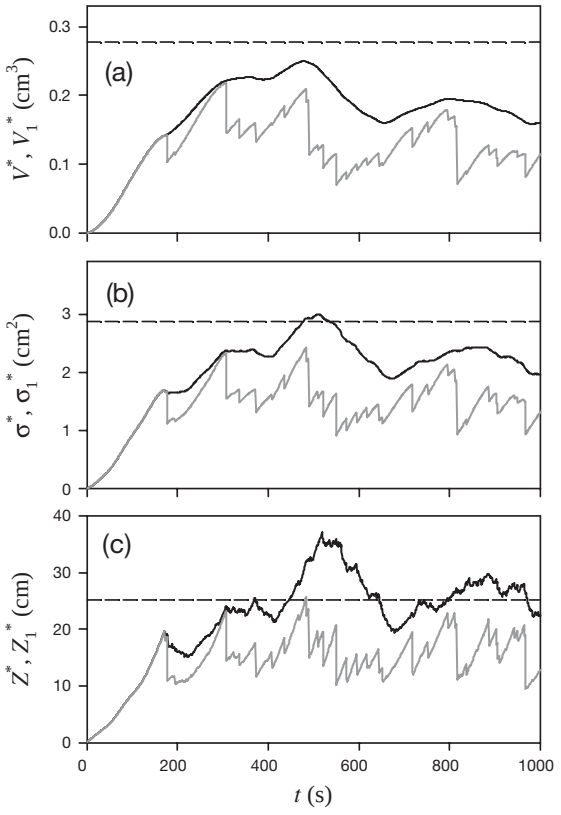

Fig. 3. (a) Plume volume, (b) plume cross section and (c) plume length for a marine snow particle (r = 0.1 cm, w = 0.07 cm s^{-1}, $L = 3 \times 10^{-14}$ mol s^{-1}, $C^* = 10^{-11}$ mol cm^{-3}) under turbulent conditions ($\varepsilon = 10^{-4}$ cm^2 s^{-3}, I = 100 cm) as a function of time. Total plume metrics are shown in black, whereas plume metrics associated with the 1st connected plume segment are shown in grey. Dashed lines represent the non-turbulent values of Z_0^* (a), σ_0^* (b) and V_0^* (c)

which is equivalent to the plume length for no turbulent straining. Use of Eq. (A1-15) yields the radial distance at which the plume can be detected as:

$$\rho^{*2} = \frac{4D\xi}{\xi\gamma + w}\ln\left(\frac{Z_0^*}{\xi}\right) \quad (24)$$

The volume of the plume is thus given by:

$$V^* = \pi\int_0^{Z_0^*}(\rho^*(\xi))^2 d\xi = 4V_0^*\int_0^1 \frac{\xi'}{\gamma T_0^* + \xi'}\ln(\xi')d\xi' \quad (25)$$

where $\xi' = \xi/Z_0^*$. The integral does not yield an analytic solution, although it can be numerically solved. In a similar manner, the cross sectional area can be computed as:

$$\sigma^* = 2\int_0^{Z_0^*}\rho^*(\xi)d\xi = \rho_0^*\sqrt{\frac{27}{2\pi}}\int_0^1\left[-\frac{\xi'}{\gamma T_0^* + \xi'}\ln(\xi')\right]^{1/2} d\xi' \quad (26)$$

Numerical evaluations of the theoretical predictions from Eqs. (25) & (26) show that they are essentially the

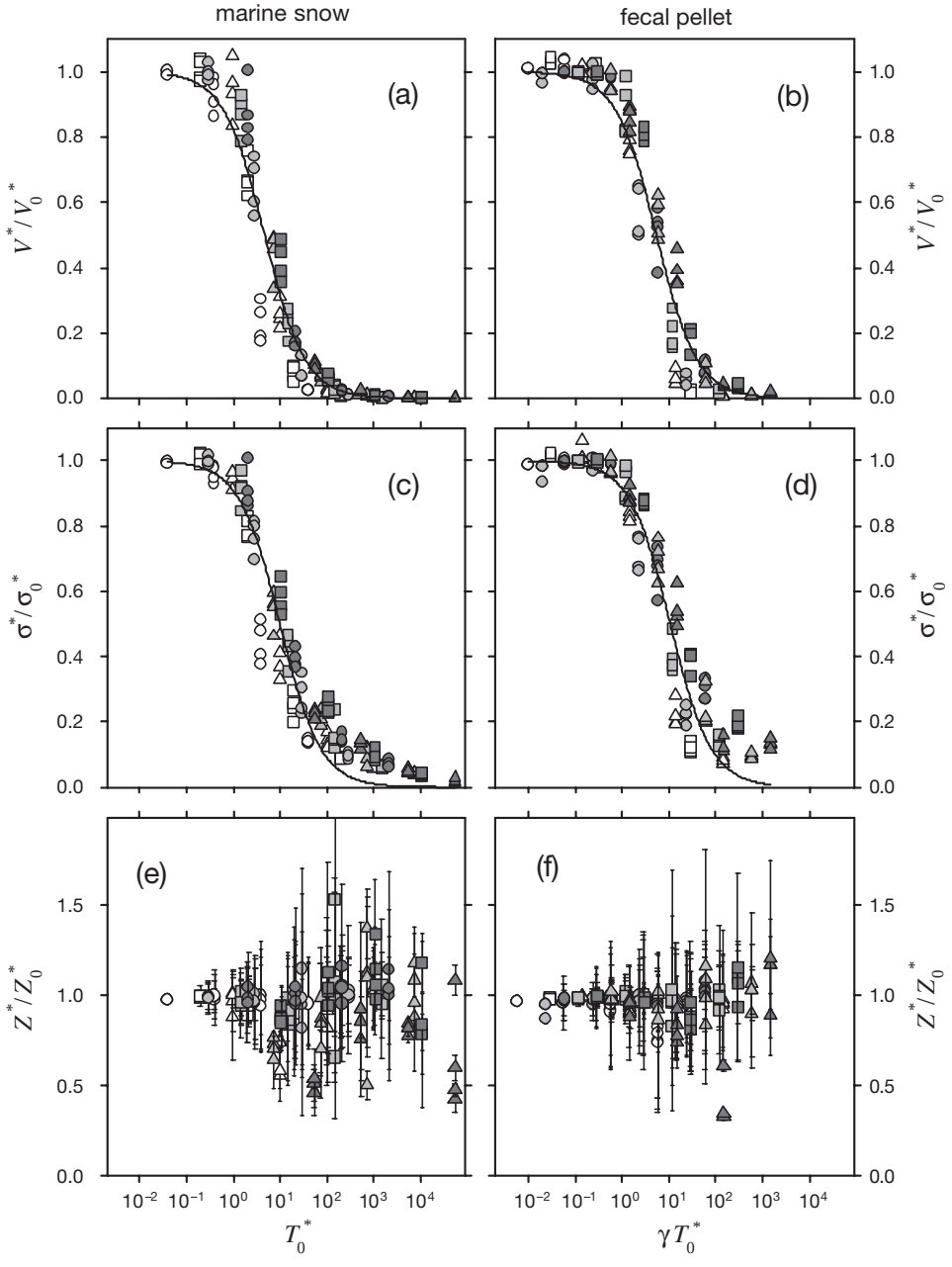

Fig. 4. Normalized total plume metrics as a function of the scaled mean turbulent rate of strain γT_0^*. Metrics are (a,b) plume volume, (c,d) plume cross-sectional area and (e,f) plume length. Representative values were used for (a,c,e) marine snow and (b,d,f) fecal pellets. The best fit reciprocal function Eq. (21) is drawn for (a–d) and fit parameters listed in Table 3. Symbols indicate different threshold concentrations C^* [mol cm^{-3}] (○ = 5×10^{-11}, Δ = 1×10^{-11}, □ = 2×10^{-12}) and shading indicates different particle sizes: marine snow r [cm] (white = 0.02, light grey = 0.1, dark grey = 0.5) and fecal pellets r [cm] (white = 0.002, light grey = 0.008, dark grey = 0.02)

same as those calculated by fitting Eq. (21) (Table 3) to the result of the simulations for values of a representative of marine snow and fecal pellets (Fig. 5).

First segment metrics

Simulation results. For the first segment, that closest to the particle, the volume V_1^* and the cross-sectional area σ_1^* depend on turbulent intensity in ways similar to those for the corresponding values for the total plume (Fig. 6a–d). V_1^* and σ_1^* can also be fit to equations of the form of Eq. (21) (Table 3).

There are 2 different measures of the first segment length, the straight-line distance between particle and plume end X_1^*, and the along-plume distance between the two Z_1^* (Fig. 7), that show different relationships to turbulent intensity. X_1^* is similar to V_1^* and σ_1^* (Fig. 6e,f) and can be fit to Eq. (21) (Table 3). This relationship is expected because $X_1^* \approx wT^*$, which from Eq. (22) gives:

$$\frac{X_1^*}{Z_0^*} \approx \frac{\ln\left(\gamma T_0^* + 1\right)}{\gamma T_0^*} \approx \frac{1}{1 + 0.5\gamma T_0^*} \qquad (27)$$

The coefficient 0.5 suggested by this analysis is very close to the values found by fitting the simulation

Table 3. Best fit parameters for the normalized plume metrics to the reciprocal function $f = 1/(1 + a\gamma T_0^*)$. For Z_1^*, the form of the function is $h = (1 + b\gamma T_0^*)/(1 + a\gamma T_0^*)$

		l (cm)	Fit parameter(s)		SE	R^2
Total plume						
V^*	Marine snow	100	a	0.22	0.02	0.95
	Fecal pellet	100	a	0.19	0.01	0.96
	Marine snow	1000	a	0.28	0.02	0.94
σ^*	Marine snow	100	a	0.10	0.01	0.94
	Fecal pellet	100	a	0.09	0.01	0.96
	Marine snow	1000	a	0.11	0.01	0.92
Connected plume						
V_1^*	Marine snow	100	a	0.30	0.02	0.95
	Fecal pellet	100	a	0.29	0.02	0.97
	Marine snow	1000	a	0.40	0.02	0.95
σ_1^*	Marine snow	100	a	0.20	0.01	0.96
	Fecal pellet	100	a	0.21	0.01	0.97
	Marine snow	1000	a	0.26	0.03	0.95
X_1^*	Marine snow	100	a	0.29	0.01	0.97
	Fecal pellet	100	a	0.37	0.02	0.96
Z_1^*	Marine snow	100	a	0.21	0.05	0.63
		100	b	0.43	0.09	
	Fecal pellet	100	a	0.31	0.06	0.72
		100	b	0.59	0.11	

results to particles typical of marine snow and of fecal pellets (Table 3).

The value of Z_1^* has a somewhat different dependence on turbulence (Fig. 6g,h). For short times before the plume fully develops ($\gamma T_0^* \ll 1$), $Z_1^* \approx Z_0^* \approx Z^*$. However, once the plume is fully established ($\gamma T_0^* \gg 1$), $Z_1^* \approx \frac{1}{2} Z_0^*$, albeit with considerable variability. Since $Z_0^* \approx Z^*$, the first segment tends to be about half the total length of the plume in high turbulence. In this case, a more appropriate empirical fit is (Fig. 6g,h & Table 3):

$$Z_1^* = Z_0^* \frac{1 + b\gamma T_0^*}{1 + a\gamma T_0^*} \tag{28}$$

Theoretical justification. The material line plume length Z_1^* and the Euclidean plume length X_1^* have quite distinct properties as turbulence increases: X_1^* becomes much less than Z_0^*, whereas Z_1^* remains finite and tends to $\frac{1}{2} Z_0^*$. Physically, this means that the plume becomes more and more contorted with increasing turbulence (Fig. 7). In addition, the rate of strain is variable (Appendix 3), implying that somewhere along the plume length, some segments will experience a strain rate greater than the mean γ. The concentration of such a segment drops below the threshold (breaks the plume) sooner than segments with lower average strain rates. The time scale for this segment to become undetectable is (Eq. 22):

$$T_m^* = \frac{1}{c\gamma} \ln\left(c\gamma T_0^* + 1\right) \tag{29}$$

where $c\gamma$ is the average strain rate for the 'breaking' segment. The length of the plume to the first break is given by $Z_1 \approx \xi(T_m)$, which from Eq. (A2-4) gives:

$$Z_1^* = \frac{Z_0^*}{\gamma T_0^*} \left[\left(c\gamma T_0^* + 1\right)^{1/c} - 1 \right] \tag{30}$$

That is, when $\gamma T_0^* \ll 1$, $Z_1^* \approx Z_0^*$ and the along-plume length decreases as turbulence increases.

As turbulence increases further, however, the plume becomes more contorted and fills a smaller region of space. When its Euclidean length scale becomes smaller than the Taylor microscale λ_T, the entire plume experiences essentially the same rate of strain at a given time (Fig. 7). Thus, there is a lower size limit (i.e. upper turbulence limit) where Eq. (30) holds, beyond which the plume length varies less with increasing turbulence.

Disconnected signal. While the cross section area σ_1^* and volume V_1^* of the first plume segment have the same functional response to turbulence as the total plume, they decrease somewhat faster with increasing turbulence. This is not surprising, since the first plume segment should always have a smaller cross section and volume than the total plume. The ratios σ_1^*/σ^* and V_1^*/V^* have the same form as Eq. (28), and approach a ratio of about 0.5 for large values of γT_0^*. This can be seen from the best fit parameters in Table 3. That is, as turbulence increases, only half of the plume, as measured by its length, volume or cross-sectional area, is connected to the sinking particle itself. While a break should not affect bacteria consuming dissolved material, it could interfere with animals searching for the particle if a significant proportion of detected signal is spurious with no promised meal at the end.

How spurious detected signals are depends on how many breaks there are along the length of the plume, the Euclidean (straight line) distances of the inter-

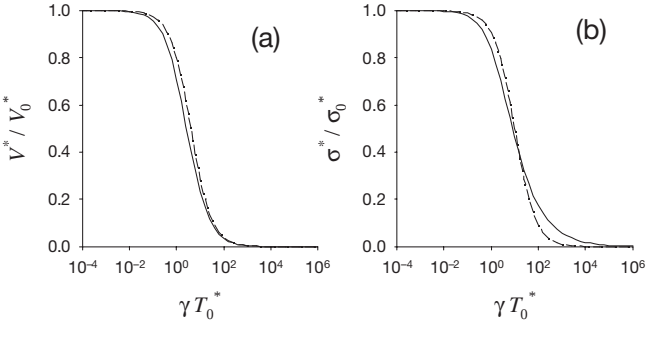

Fig. 5. Normalized (a) total plume volume and (b) cross-section area as a function of turbulent rate of strain. Solid line: values estimated using theoretical Eqs. (25) & (26); dashed line: values estimated from simulation results (Eq. 21, Table 3). Value of $a = 0.25$ for volume (a) and $a = 0.25$ for cross sectional area (b)

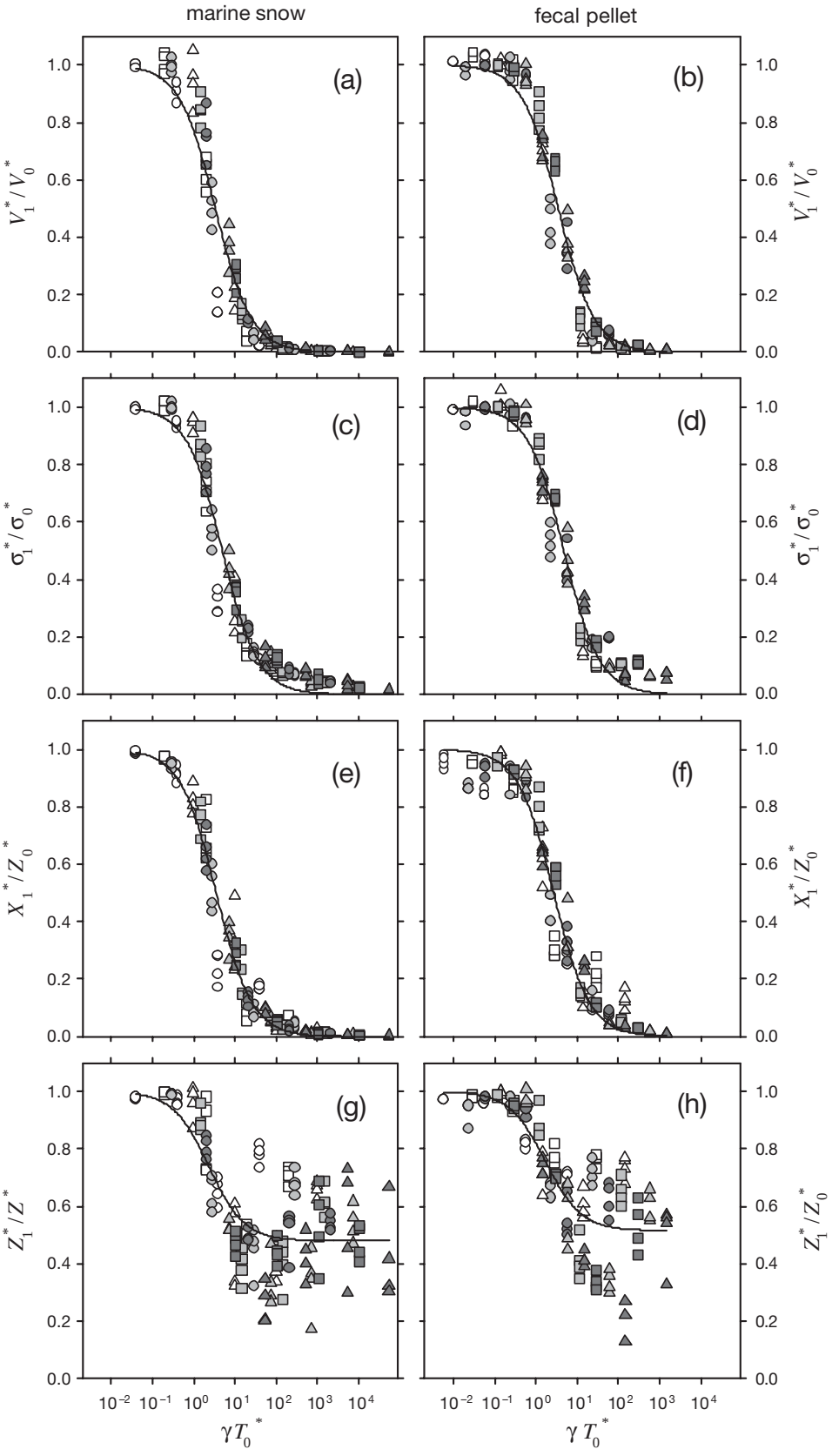

Fig. 6. Normalized plume metrics for the connected portion of the plume. Plume volume (a) marine snow and (b) fecal pellet. Plume cross sectional area (c) marine snow and (d) fecal pellet. Euclidean plume length (e) marine snow and (f) fecal pellet and material line plume length (g) marine snow and (h) fecal pellet. The best fit reciprocal function Eq. (22) is drawn for (a–h) and fit parameters listed in Table 3. Symbols and shading indicate threshold concentration and particle size as in Fig. 4

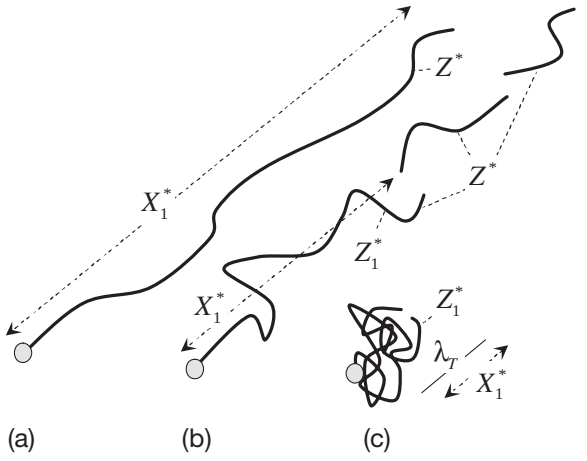

Fig. 7. Schematic representation of plume length metrics as a function of γT_0^*. (a) For low γT_0^* diffusion dominates and $Z_0^* \approx Z_1^* \approx X_1^*$. (b) At intermediate levels both diffusion and straining are important and $Z_0^* > Z_1^* > X_1^*$. (c) At high levels the plume becomes contorted and $Z_1^* \approx \frac{1}{2}Z_0^* \gg X_1^* \approx \lambda_T$

spersed gaps and the behavioural response of animals. The length of the first gap x_1^* tends to be largest for midrange turbulence levels, $0.1 < \gamma T_0^* < 10$ (Fig. 8). Below this turbulence range, diffusion dominates and few gaps exist. Beyond this range, the plume becomes contorted and fills a smaller space. Any gaps that do appear are confined to this space. There is, however, a great deal of variability in these results, part of which may be explained by dependencies on particle size and threshold concentration. Closer examination of the source of this variability is beyond the scope of this present work.

Effect of integral length scale

The integral length scale I is an important property of turbulent fields. It represents the scale of the largest turbulent motions. Despite this importance, it has relatively little impact on the primary plumes because their lengths tend to be smaller than I. Changing the integral length scale from 100 to 1000 cm has a relatively small effect on the plume metrics (Table 3). The value of the parameter a changes from 0.22 ± 0.02 to 0.28 ± 0.02 for V^* and from 0.30 ± 0.02 0.40 ± 0.02 for V_1^*. The relative differences are smaller for σ^* and σ_1^*.

DISCUSSION

One of the surprising results of this analysis is the simplicity of the descriptions of plume properties in terms of non-turbulent properties and correction factors that are simple functions of γT_0^* (Fig. 9). The results for the 2 different types of particle we tested, representative of marine snow and of fecal pellets, are essentially the same (Table 3). One way to describe the conditions at which a turbulence correction factor becomes important is the turbulent intensity at which the factor equals 0.5. For the correction factors having the form of Eq. (21), this occurs for $\gamma T_0^* = a^{-1}$. For the values of a in Table 3, this half-value is in the range $\gamma T_0^* = 2.5–11$. As a result, the turbulence correction for plume properties is small for $\gamma T_0^* < 2$.

More systematically, the effect of turbulence can be examined for a range of particle sizes. Jackson & Kiørboe (2004) examined the plume length as a function of particle radius for particles typical of marine snow and of fecal pellets. The absolute values of the plume metrics calculated using the results in Table 3 show that the effect of turbulence is strongly dependent on particle size (Fig. 10). For instance, at low turbulence levels $V \propto r^{2.5}$ and $V \propto r^4$ approximately for marine snow and fecal

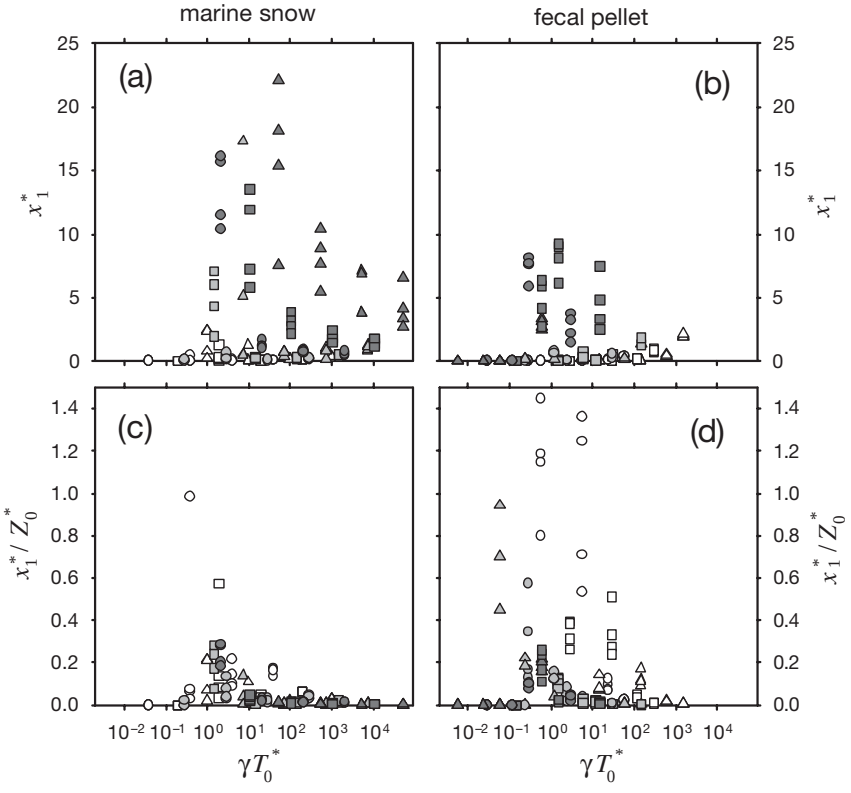

Fig. 8. (a,b) Length x_1^* in cm and (c,d) normalized length x_1^*/ Z_0^* of the 1st gap of the plume as a function of γT_0^* for (a,c) marine snow and (b,d) fecal pellets. Symbols and shading indicate detection threshold and particle size as given in Fig. 4

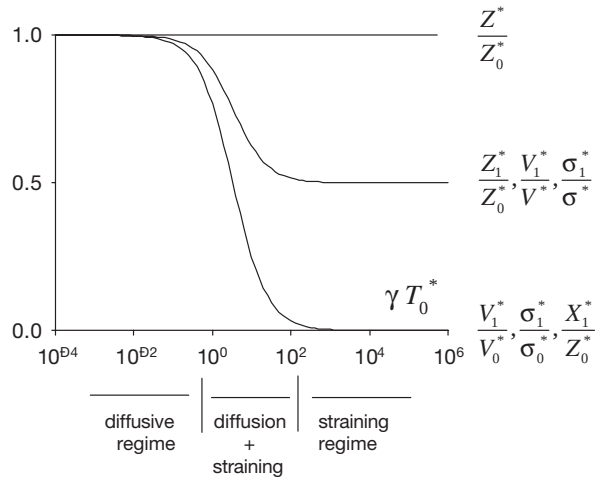

Fig. 9. Summary sketch of the various plume metrics and how they vary with turbulence

pellets, respectively. This power dependence decreases with increasing turbulence. Plumes associated with larger particles are relatively more susceptible to the effects of turbulence than those associated with smaller particles. For a marine snow particle of 1 cm, all plume metrics decrease by about 3 orders of magnitude with turbulence increasing from 10^{-6} to 1 cm^2 s^{-3} (Fig. 10). In comparison, the effects of turbulence is less dramatic for fecal pellets where plume characteristics vary only by 1 order of magnitude over the same turbulence range.

Jackson & Kiørboe (2003) argued that the rates of chemo-detection of a plume should be greater than detection by hydrodynamic means for larger particles. The results for turbulence have shown that it decreases the effective size of the plumes of larger particles more than those of smaller particles. As a result, turbulence counteracts the advantage of using chemical plumes to find larger particles in the turbulent upper layer.

Vertical differentiation

The large effect that turbulence intensity can have on the plume characteristics greatly affects the ability of an animal to find a plume or the period that a plume lasts as an identifiable entity. The strong vertical gradients in energy dissipation rates (e.g. Yamazaki et al. 2002) suggest that different modes of particle finding are favoured at different depths. Near the surface, the eddy dissipation rates are typically 10^{-2} to 1 cm^2 s^{-3}, large enough to greatly diminish plume properties (Fig. 10). By a depth of 50 m, ε is typically in the range 10^{-6} to 10^{-4} cm^2 s^{-3}, a range where the effect on plume properties is relatively small (Fig. 10).

The differences in plume detectability, even over such relatively small vertical distances as 50 m, and the relative advantages of different means of detecting particles suggests that these environments favour different modes of feeding. The issue is made more complex by the temporal variability in surface wind forcing associated with the increased values of ε near the surface. In the absence of such forcing, however, the value of ε is not that different from values deeper in the water column. Thus, the relative advantage of different particle detection modes is not constant even at a single depth.

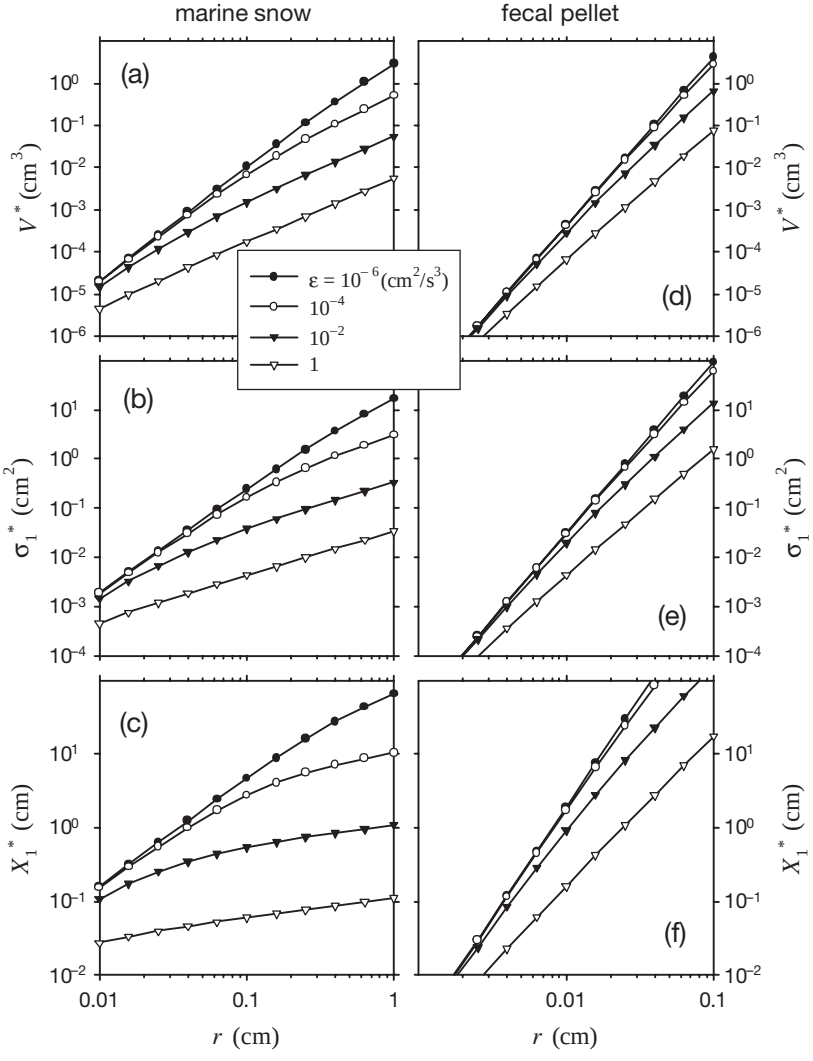

Fig. 10. Effect of particle size on various metrics for different turbulence intensities. Particle sizes are typical for (a,c,e) marine snow and (b,d,f) fecal pellets. Values of ε = 10^{-6}, 10^{-4}, 10^{-2}, 1 cm^2 s^{-3}

Examples

Excretion from a swimming copepod. Several years ago, there was discussion of the importance of non-uniform regeneration of nutrients, such as that resulting from excretion by a swimming copepod (e.g. Goldman et al. 1979, Jackson 1980, Lehman & Scavia 1982, Jackson 1987). Any plume left by such a copepod would be subject to the same processes as the plume behind a falling particle. For the numbers in Jackson (1980), $w = 1200$ m d^{-1} = 1.4 cm s^{-1}, and a filtration rate of 168 cm^3 d^{-1}, and assuming that the animals convert 0.1 µM = 10^{-10} mol cm^{-3}, then the copepods release at a rate equivalent to $L = 1.94 \times 10^{-13}$ mol s^{-1}. Assuming that a background concentration of 10^{-11} mol cm^{-3} is an appropriate value for C^*, then $Z_0^* = 154$ cm and $T_0^* = 135$ s. The plume will be decreased if $\gamma T_0^* \approx 2$ or $\varepsilon \approx 10^{-6}$ cm^2 s^{-3}. Because the surface mixed layer has greater turbulence, there will be a dramatic decrease in plume extent and lifetime near the surface.

Discarded appendicularian houses and their encounter by copepods. Appendicularians, also known as larvaceans, are common members of many marine pelagic ecosystems and can reach abundances of $C_a = 300$ m^{-3} over the upper 10 m (Vargas et al. 2002). They construct a mucus housing through which they filter seawater. The filters become clogged with time, forcing animals to abandon the old and build new houses, typically every $T_h = 4$ to 6 h (Hansen et al. 1996). The abandoned houses can form a significant fraction of the particulate mass settling out of the surface layer, either by themselves or as part of mixed aggregates. Typical appendicularian houses (e.g. *Oikopleuria dioica*, *Fritillaria borealis*) are 0.2 cm in radius, which corresponds to a sinking speed of $w = 0.08$ cm s^{-1} (=74 m d^{-1}) and a leakage rate of $L = 9 \times 10^{-14}$ mol s^{-1} (Eq. 8 in Kiørboe & Thygesen 2001). At a threshold detection concentration of $C^* = 10^{-11}$ mol cm^{-3}, this gives a plume length of $Z_0^* = 70$ cm (Eq. 1) and a detection time scale $T_0^* = 830$ s in still water (Eq. 5). In still water, the plume volume (Fig. 11a) is 1.8 cm^3 and is of the same magnitude, 1.1 cm^2 at low turbulence levels ($\varepsilon = 10^{-6}$ cm^2 s^{-3}). However, at moderately high turbulence levels ($\varepsilon = 10^{-2}$ cm^2 s^{-3}), the volume is reduced to 0.02 cm^3, nearly 2 orders of magnitude. A similar reduction range is seen in other plume metrics (Fig. 11b,c) and is bound to a have significant impact on the encounter rate between discarded house aggregates and colonizing organisms.

Fecal pellets. Solute plumes associated with typical fecal pellets are much shorter and have a smaller diffusion time scale associated with them than typical marine snow aggregates. Even for relatively large fecal pellets such as for *Calanus finmarchicus* (equivalent spherical radius $r = 0.008$ cm), the plume length is $Z_0^* = 5$ cm and the effects of turbulence come into play

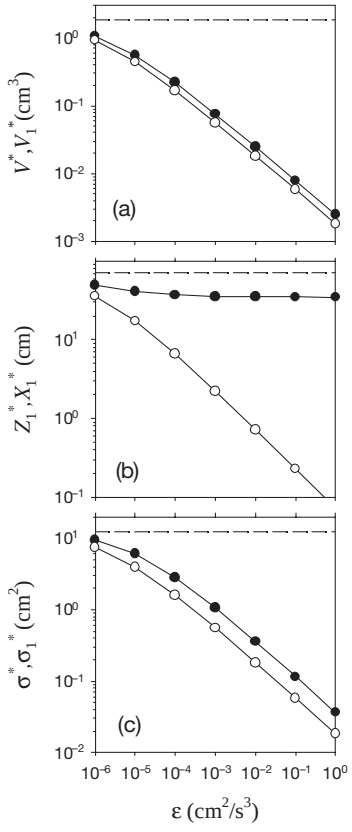

Fig. 11. Plume metrics as a function of turbulent dissipation rate for a marine snow aggregate of size $r = 2$ mm and detection threshold $C^* = 10^{-11}$ mol cm^{-3}. The dashed line indicates the metric value for calm water, (a) plume volume (● total, ○ 1st segment), (b) plume length (● 1st segment along plume, ○ 1st segment Euclidean) and (c) plume cross section (● total, ○ 1st segment)

at $\varepsilon > 10^{-4}$ cm^2 s^{-3}, a moderately high turbulence level. Diffusive time scales T^* range from 10 s at 10^{-6} cm^2 s^{-3} to 0.5 s at 1 cm^2 s^{-3} suggesting that solute rapidly diffuse below detection levels. For smaller pellets (e.g. *Acartia tonsa*, $r = 0.004$ cm), $Z_0^* = 1$ cm and turbulence effects appear at $\varepsilon > 10^{-3}$ cm^2 s^{-3}. The relative importance of plume detection versus hydromechanical signals has been considered by Jackson & Kiørboe (2004) who showed that for fecal pellets in still water, the encounter rate mediated by the 2 detection mechanisms were of similar magnitude. This finding may be qualitatively invariant under turbulence given that turbulence effects only appear at relatively high levels and that at these levels hydromechanical signal detection would also be compromised (e.g. Visser 2001).

Unresolved issues

In presenting these results, we have focused on those aspects that have relatively robust statistics. In

doing so we have glossed over many aspects leading to variability in the various measures of plumes and their contribution to the spatial homogeneity of the pelagic environment. For example, turbulence makes the plume cross-section compact and overlapping rather than elongate. The fact that the straight line distance to a particle is significantly shorter than the along plume length could have implications for zooplankton behaviour in turbulent environments.

The signal. The sensing ability of animals is an important but largely unknown aspect of the total problem of finding particles by the use of plumes. For instance, the nature of the chemical being sensed (Carr 1988, Zimmer & Butman 2004), the sensitivity of animals and signal strength above background levels (e.g. Hamner & Hamner 1977, Poulet & Ouellet 1982, Atema 1988) are all important issues with regards plume detection.

Behaviour. Likewise, behavioural aspects of how animals follow chemical trails (e.g. Hamner & Hamner 1977, Yen et al. 1998, Tsuda & Miller 1998) are important in utilizing information. Because the concentration gradient along a plume is very small, there are no simple chemical cues telling an animal which direction to choose when it finds the trail. Observations show that animals have a significant probability of choosing the wrong direction when tracking a plume (e.g. Kiørboe 2001), but they reverse directions when they discover their error. The behavioural response of animals to plume breaks (Hamner & Hamner 1977) and the efficiency their subsequent search strategy will impact finding particles, particularly when turbulent intensity is high. Finally, there is the spatial complexity of a plume and how animals react to it (e.g. Yen et al. 1998, Tsuda & Miller 1998, Yen et al. 1998). The interpretation of the plume size implicitly assumes that the plume is laid out in a way that does not have it folding over itself. However, the compact nature of the plume, as shown by the difference between along-plume length of a plume and the straight line distance suggests that there can be a significant decrease in actual cross-sectional area.

Multiple particles. The actual environment that a zooplankter or bacterium experiences is the result of many particles of different sizes and sinking speeds falling around it. One way to incorporate this particle diversity is to use multiple particles consistent with an observed particle size spectrum, as was done in Jackson & Kiørboe (2004). To what extent do plumes from small particles mask signals from larger ones creating spurious signatures?

Turbulence. Finally, certain issues regarding the kinematic simulations and turbulence as seen in the marine environment remain unresolved. Firstly, the simulations proceed on the assumption that marine turbulence is isotropic: often it is not. Because of stratification, vertical turbulent motions are damped out more rapidly than horizontal components and isotropic conditions are met for only smaller scales of the turbulent motion (e.g. Gargett et al. 1984). In addition, the kinematic simulations used here share only some of the characteristics of fully developed isotropic 3D turbulence (e.g. Fung et al. 1992, Yamazaki et al. 2004). The important nonlinear processes that establish the phase relationship between scales are not captured. As a result, coherent structures are absent in the kinematic simulations. Also, the mean principal rates of strain, i.e. the mean eigenvalues of the rate of strain tensor, have the ratio (1:0:–1) (–ve indicating compression, +ve extension) in the kinematic simulations, whereas in turbulence, they appear as ($\frac{3}{4}$:$\frac{1}{4}$:–1) both in observations (Smyth 1999) and direct numerical simulations (Yamazaki et al. 2004). Since straining plays a central role in the development of the plume, this difference may have some impact on the results reported here.

Conclusion

The characteristics of a chemical plume exuded from a moving source in a turbulent water column is a generic problem in the pelagic environment. Such considerations are important in the encounter rate of chemosensory organisms with sinking marine snow particles and fecal pellets, a process central in the remineralization of organic carbon produced in the euphotic zone. Similar considerations hold in determining the encounter rate of male copepods with pheromone trails released by swimming females. Depending on the details of the encounter process, the relevant plume metrics are the detectable plume volume, plume cross sectional area and plume length. Despite the complexity of the parameter space involved, particle size-dependent sinking and leakage rates, species-dependent detection thresholds as well as highly variable turbulence levels, the form of these plume metrics appear to conform to simple functional relationships. Armed with these functional relationships, it is possible to translate observed particle size spectra into spectra of dissolved organic matter patches in pelagic environments.

Acknowledgements. This work was supported by grants OCE9986765, OCE9981424 and OCE0097296 from US-JGOFS program in the Ocean Sciences Division of NSF (GAJ), and the Danish Natural Science Research Council, contract # 21-01-0549 (AWV), and by the SLIP research school under the Danish Network for Fisheries and Aquaculture Research (www.fishnet.dk) financed by the Danish Ministry for Food, Agriculture and Fisheries and the Danish Agricultural and Veterinary Research Council. T. Kiørboe and U. Thygsen provided surprisingly useful input and advice.

LITERATURE CITED

Alldredge AL (1998) The carbon content, nitrogen and mass content of marine snow as a function of aggregate size. Deep-Sea Res 45:529–541

Alldredge AL, Gotschalk CC (1988) *In situ* settling behavior of marine snow. Limnol Oceanogr 33:339–351

Alldredge AL, Gotschalk CC (1989) Direct observations of the mass flocculation of diatom blooms: characteristic settling velocity and formation of diatom aggregates. Deep-Sea Res 36:159–171

Atema J (1988) Distribution of chemical stimuli. In: Atema J, Fay RR, Popper AN, Tavolga WN (eds) Sensory biology of aquatic organisms. Springer-Verlag, New York, p 29–56

Batchelor GK (1952) The effect of homogeneous turbulence on material lines and surfaces. Proc R Soc Lond A 213: 349–366

Batchelor GK (1959) Small scale variation of convected quantities like temperature in a turbulent fluid. Part 1. General discussion and the case of small conductivity. J Fluid Mech 6:113–133

Bowen JD, Stolzenbach KD, Chisholm SW (1993) Simulating bacterial clustering around phytoplankton cells in a turbulent ocean. Limnol Oceanogr 38:36–51

Carlucci AF, Craven BD, Robertson KJ, Henrichs SM (1986) Microheterotrophic utilization of dissovled free amino acids in depth profiles of the Southern California Borderland basin waters. Oceanol Acta 9:89–96

Carr WES (1988) The molecular nature of chemical stimuli in the aquatic environment. In: Atema J, Fay RR, Popper AN, Tavolga WN (eds) Sensory biology of aquatic animals. Springer-Verlag, Berlin, p 3–27

Carslaw HS, Jaeger JC (1959) Conduction of heat in solids. Oxford University Press, Oxford

Cocke WJ (1969) Turbulent hydrodynamic line stretching: consequences of isotropy. Phys Fluids 12:2488–2492

Fung JCH (1993) Gravitational settling of particles and bubbles in homogeneous turbulence. J Geophys Res 98: 20287–20297

Fung JCH (1998) The effect of nonlinear drag on the settling velocity of particles in homogeneous isotropic turbulence. J Geophys Res 103:27905–27917

Fung JCH, Hunt JCR, Malik NA, Perkins RJ (1992) Kinematic simulation of homogeneous turbulence by unsteady random Fourier modes. J Fluid Mech 236:281–318

Fung JCH, Vassilicos JC (1998) Two-particle dispersion in turbulent like flows. Phys Rev E 57:1677–1690

Gargett AE (1997) 'Theories' and techniques for observing turbulence in the ocean euphotic zone. Sci Mar 61:25–45

Gargett AE, Osborn TR, Nasmyth PW (1984) Local isotropy and the decay of turbulence in a stratified fluid. J Fluid Mech 144:231–280

Gavis J (1976) Munk and Riley revisited: nutrient diffusion, transport and rates of phytoplankton growth. J Mar Res 34:161–179

Girimaji SS, Pope SB (1990) Material element deformation in isotropic turbulence. J Fluid Mech 220:427–458

Goldman JC, McCarthy JJ, Peavey DG (1979) Growth-rate influence on the chemical composition of phytoplankton in oceanic waters. Nature 279:210–215

Hamner P, Hamner WM (1977) Chemosensory tracking of scent trails by the planktonic shrimp *Acetes sibogae australis*. Science 195:886–888

Hansen JLS, Kiørboe T, Alldredge AL (1996) Marine snow derived from abandoned larvacean houses: sinking rates, particle content and mechanisms of aggregate formation. Mar Ecol Prog Ser 141:205–215

Jackson GA (1980) Phytoplankton growth and zooplankton grazing in oligitrophic oceans. Nature 284:439–441

Jackson GA (1987) Physical and chemical properties of aquatic environments. In: Fletcher M, Gray TRG, Jones JG (eds) Ecology of microbial communities. Cambridge University Press, Cambridge, p 213–233

Jackson GA (1989) Simulation of bacterial attraction and adhesion to falling particles in an aquatic environment. Limnol Oceanogr 34:514–530

Jackson GA, Burd AB (1998) Aggregation in the marine environment. Environmental Science & Technology 32: 2805–2814

Jackson GA, Kiørboe T (2004) Zooplankton use of chemodetection to find and eat particles. Mar Ecol Prog Ser 269: 153–132

Jiang H, Meneveau C, Osborn TR (2002) The flow field around a freely swimming copepod in steady motion: Part II numerical simulation. J Plankton Res 24:191–213

Karp-Boss L, Boss E, Jumars PA (1996) Nutrient fluxes to planktonic osmotrophs in the presence of fluid motion. Oceanogr Mar Biol 34:71–107

Kiørboe T (2001) Formation and fate of marine snow: small-scale processes with large-scale implications. Sci Mar 65: 57–71

Kiørboe T, Ploug H, Thygesen UH (2001) Fluid motion and solute distribution around sinking aggregates. I. Small-scale fluxes and heterogeneity of nutrients in the pelagic environment. Mar Ecol Prog Ser 211:1–13

Kiørboe T, Thygesen UH (2001) Fluid motion and solute distribution around sinking aggregates. II. Implication for remote detection by colonizing zooplankters. Mar Ecol Prog Ser 211:15–25

Kiørboe T, Visser AW (1999) Predator and prey perception in copepods due to hydromechanical signals. Mar Ecol Prog Ser 179:81–95

Kraichnan RH (1970) Diffusion by a random velocity field. Phys Fluids 13:22–31

Lazier JRN, Mann KH (1989) Turbulence and the diffusive layers around small organisms. Deep-Sea Res 36: 1721–1733

Lehman JT, Scavia D (1982) Microscale nutrient patches produced by zooplankton. Proc Nat Acad Sci USA 79: 5001–5005

Lewis DM, Pedley TJ (2000) Planktonic contact rates in homogeneous isotropic turbulence: theoretical predictions and kinematic simulations. J Theor Biol 205: 377–408

Lewis DM, Pedley TJ (2001) The influence of turbulence on plankton predation strategies. J Theor Biol 210:347–365

Maar M, Nielsen TG, Stips A, Visser AW (2003) Microscale distribution of zooplankton in relation to turbulent diffusion. Limnol Oceanogr 48:1312–1325

Malik NA, Vassilicos JC (1999) A Lagrangian model for turbulent dispersion with turbulent-like flow structure: comparison with direct numerical simulation for two-particle statistics. Phys Fluids 11:1572–1580

Monin P, Yaglom AM (1975) Statistical fluid mechanics. MIT Press, Cambridge, MA

Munk W, Riley GA (1952) Absorbtion of nutrients by aquatic plants. J Mar Res 11:215–240

Okubo A (1980) Diffusion and ecological problems: Mathematical models. Springer-Verlag, Berlin

Poulet SA, Ouellet G (1982) The role of amino acids in the chemosensory swarming and feeding of marine copepods. J Plankton Res 4:341–361

Poulet SA, Williams R, Conway DVP, Videau C (1991) Co-occurrence of copepods and dissolved free amino acids in

shelf waters. Mar Biol 108:373–385
Rothschild BJ, Osborn TR (1988) Small-scale turbulence and plankton contact rates. J Plankton Res 10:465–474
Small LF, Fowler SW, Ünlü MY (1979) Sinking rates of natural copepod fecal pellets. Mar Biol 51:233–241
Smyth WD (1999) Dissipation-range geometry and scalar spectra in sheared stratified turbulence. J Fluid Mech 401:209–242

Appendix 1. Length and detection of a plume under turbulent straining

The concentration field associated with diffusion from a line source is given by:

$$\phi(\rho,t) = \frac{q}{4\pi Dt} e^{-\rho^2/(4Dt)} \quad \text{(A1-1)}$$

(Carslaw & Jaeger 1959) where ρ is the radial distance to the line source, q is the source strength in units of mass per unit length and D is the molecular diffusivity. This result is equivalent to the solution for the concentration behind a point source moving at a velocity w at a distance z ($=wt$) behind the source:

$$\phi(\rho,z) = \frac{L}{4\pi Dt} e^{-\rho^2 w/(4Dz)} \quad \text{(A1-2)}$$

where L ($=wq$) is the leakage rate in units of mass per time (Okubo 1980, Jackson & Kiørboe 2003). After a short time step δ, the concentration field is given by:

$$\phi(\rho,\delta) = \frac{L}{4\pi Dw\delta} e^{-\rho^2/(4D\delta)} \quad \text{(A1-3)}$$

consistent with the initial conditions set on $C_{i,j}$ and $\lambda_{i,j}$ in Eqs. (17) & (18).

Consider a cylinder of infinitesimal length ξ_i, radius ρ_i and volume $\pi\xi_i\rho_i^2$. Because the length is $\xi_{i+1}=\xi_i e^{-\gamma\delta}$ after stretching over a short time step δ with mean uniform rate of strain γ, conservation of mass implies that $\rho_{i+1}^2 = \rho_i^2 e^{-\gamma\delta}$. As a result, for a chemical tracer initially distributed as a Gaussian cylindrical distribution (Eq. 14), both straining of the fluid along the central axis and diffusion perpendicular to it transform one Gaussian distribution to another. In particular, if the initial distribution at a particular time is:

$$\phi_i = C_i \exp\left(-\frac{\rho^2}{\lambda_i^2}\right) \quad \text{(A1-4)}$$

then stretching over time δ means the positions of the resulting concentrations are described by:

$$\phi_{i+1}^s = C_i \exp\left(-\frac{\rho^2}{\lambda_i^2 e^{\gamma\delta}}\right) \quad \text{(A1-5)}$$

A comparison of Eq. (A1-4) with that for pure diffusion, Eq. (A1-1), shows that the two are equivalent if $\lambda_i^2 = 4Dt_i$ and $C_i = q/\pi\lambda_i^2$. For $t = t_i + \delta$, Eq. (A1-1) implies:

$$\phi_{i+1}^d = \frac{\lambda_i^2 C_i}{4D\delta + \lambda_i^2} \exp\left(-\frac{\rho^2}{4D\delta + \lambda_i^2}\right) \quad \text{(A1-6)}$$

To incorporate both processes, we incorporate the expression for λ_{i+1}^2 from Eq. (A1-5) into Eq. (A1-6) for a short time step δ:

$$\phi_{i+1} = \frac{\lambda_i^2 C_i e^{-\gamma\delta}}{4D\delta + \lambda_i^2 e^{-\gamma\delta}} \exp\left(-\frac{\rho^2}{4D\delta + \lambda_i^2 e^{-\gamma\delta}}\right) = C_{i+1}\exp\left(-\frac{\rho^2}{\lambda_{i+1}^2}\right) \quad \text{(A1-7)}$$

from which we deduce the recursion formulae:

$$\lambda_{i+1}^2 = 4D\delta + \lambda_i^2 e^{-\gamma\delta}$$
$$C_{i+1} = \frac{\lambda_i^2}{\lambda_{i+1}^2} C_i e^{-\gamma\delta t} \quad \text{(A1-8)}$$

These rules allow for the evaluation of $\lambda^2(t)$ and $C(t)$ in the following manner:

$$\lambda_1^2 = 4D\delta$$
$$\lambda_2^2 = 4D\delta + \lambda_1^2 e^{-\gamma\delta} = 4D\delta(1 + e^{-\gamma\delta})$$
$$\lambda_3^2 = 4D\delta + \lambda_2^2 e^{-\gamma\delta} = 4D\delta + 4D\delta(1+e^{-\gamma\delta})e^{-\gamma\delta} = 4D\delta(1+e^{-\gamma\delta}+e^{-2\gamma\delta})$$
.....
$$\lambda_n^2 = 4D\delta\sum_{i=0}^{n-1}(e^{-i\gamma\delta}) = 4D\delta\frac{1-e^{-n\gamma\delta}}{1-e^{-\gamma\delta}} \quad \text{(A1-9)}$$

Noting that $t = n\delta$, and for $\gamma\delta \ll 1$, $1-e^{-\gamma\delta} \approx \gamma\delta$, in the limit $\delta \to 0$ we get:

$$\lambda^2(t) = \frac{4D}{\gamma}(1-e^{-\gamma t}) \quad \text{(A1-10)}$$

In the limit as $\gamma \to 0$, $\lambda(t) = 2(Dt)^{1/2}$, which is the same as for the non-turbulent case. Note also that for $t \gg 1/\gamma$, the across plume length scale becomes time invariant $\lambda \approx 2(D/\gamma)^{1/2}$, which is 3 times the Batchelor scale, $\lambda_B = (D^2\nu/\varepsilon)^{1/4}$, the smallest scale of variations for a diffusing material in a turbulent flow (Batchelor 1959).

For C_i, the recursion leads to:

$$\frac{C_n}{C_{n-1}}\frac{C_{n-1}}{C_{n-2}}\cdots\frac{C_3}{C_2}\frac{C_2}{C_1} = \frac{C_n}{C_1}$$
$$= \frac{\lambda_{n-1}^2}{\lambda_n^2}\frac{\lambda_{n-2}^2}{C_{n-1}^2}\cdots\frac{\lambda_2^2}{\lambda_3^2}\frac{\lambda_1^2}{\lambda_2^2}e^{-(n-1)\gamma\delta} = \frac{\lambda_1^2}{\lambda_n^2}e^{-(n-1)\gamma\delta}$$

That is:

$$C_n = C_1\frac{\lambda_1^2}{\lambda_n^2}e^{-(n-1)\gamma\delta} \quad \text{(A1-11)}$$

The initial concentration along the axis of the plume is set by $C_1 = L/(4\pi Dw\delta)$. Thus, in the limit $\delta \to 0$:

$$C(t) = \frac{L_\gamma}{4\pi Dw}\frac{e^{-\gamma t}}{1-e^{-\gamma t}} \quad \text{(A1-12)}$$

The time evolution of a chemical tracer emitted from a sinking particle under the combined action of diffusion and a turbulent rate of strain γ is given by:

$$\phi(\rho,t) = \frac{L\gamma}{4\pi Dw}\frac{e^{-\gamma t}}{1-e^{-\gamma t}}\exp\left(-\frac{\rho^2\gamma}{4D(1-e^{-\gamma t})}\right) \quad \text{(A1-13)}$$

This can be written in terms of $\xi(t)$ using Eq. (A1-4):

$$\phi(\rho,\xi) = \frac{L}{4\pi D\xi}\exp\left(\frac{\rho^2 w}{4D\xi}\right) \quad \text{(A1-14)}$$

Note that in the limit as $\gamma \to 0$:

$$\phi_0(\rho,t) = \frac{L}{4\pi Dwt}\exp\left(-\frac{\rho^2}{4Dt}\right) \quad \text{(A1-15)}$$

as in Eq. (2) of Jackson & Kiørboe (2004).

By way of verification, it can be shown that the function $\phi(\rho,t)$ in Eq. (A1-13) is a solution to the advection-diffusion equation:

$$\frac{\partial\phi}{\partial t} = D\nabla^2\phi + \frac{\gamma}{2}\rho\nabla\phi \quad \text{(A1-16)}$$

This is in keeping with the physical prescription of the problem, an advection diffusion process (written in cylindrical coordinates) with radial advection $d\rho/dt = -\frac{1}{2}\gamma\rho$.

Suttle CA, Chan AM, Fuhrman JA (1991) Dissolved free amino acids in the Sargasso Sea: uptake and respiration rates, turnover times and concentrations. Mar Ecol Prog Ser 70:189–199

Tennekes H, Lumley JL (1972) A first course in turbulence. The MIT Press, Cambridge, MA

Tsinober A (2001) An informal introduction to turbulence. Kluwer Academic Press, Dordrecht

Tsuda A, Miller CB (1998) Mate-finding behavior in *Calanus marshallae* Frost. Phil Trans R Soc Lond B 353: 713–720

Vargas CA, Tonnesson K, Sell A, Maar M and 8 others (2002) Importance of copepods versus appendicularians in vertical carbon fluxes in a Swedish fjord. Mar Ecol Prog Ser 241:125–138

Visser AW (2001) Hydromechanical signals in the plankton. Mar Ecol Prog Ser 222:1–24

Visser AW, Saito H, Saiz E, Kiørboe T (2001) Observations of copepod feeding and vertical distribution under natural turbulent conditions in the North Sea. Mar Biol 138: 1011–1019

Yamazaki H, Mackas DL, Denman K (2002) Coupling small-scale physical processes with biology. In: Robinson AR, McCarthy JJ, Rothschild BJ (eds) Biological-physical interactions in the sea. John Wiley and Sons, New York, p 51–112

Yamazaki H, Squires KD, Strickler JR (2004) Can turbulence reduce the energy cost of hovering for planktonic organisms? In: Seuront L, Strutton PG (eds) Handbook of scaling methods in aquatic ecology. CRC Press, New York, p 493–506

Yen J, Strickler JR (1996) Advertisement and concealment in the plankton: what makes a copepod hydrodynamically conspicuous? Invert Biol 115:191–205

Yen J, Weissburg MJ, Doall MH (1998) The fluid physics of signal perception by mate-tracking copepods. Phil Trans R Soc Lond B 353:787–804

Zimmer RK, Butman CA (2004) Chemical signaling processes in the marine environment. Biol Bull 198:168–187

Appendix 2. The length of a material line

In 3D isotropic turbulence, the average distance between 2 parcels in the fluid changes at a rate that is scale-dependent. In the inertial sub-range (scales larger than the Kolmogorov length scale η and smaller than the integral length scale I), this is given by Richardson's law:

$$\frac{\partial \ell}{\partial t} = \alpha(\varepsilon \ell)^{1/3} \quad \text{(A2-1)}$$

where α is a constant of order 1, ε is the turbulent dissipation rate and ℓ describes the mean separation between any 2 points in the fluid. However, the distance between these 2 points following a material line could be considerably longer and is governed by the micro-structure rate of strain $\gamma_T = [\varepsilon/(2\nu)]^{1/2}$ associated with the turbulent flow (e.g. Batchelor 1952, Cocke 1969, Monin & Yaglom 1975, Tsinober 2001). At sub-Kolmogorov length scales, the relative distance between 2 fluid elements is given by:

$$\frac{\partial(\mathrm{d}\xi)}{\partial t} = \gamma(\mathrm{d}\xi) \text{ where } \gamma \approx \left(\frac{\varepsilon}{6\nu}\right)^{1/2} \quad \text{(A2-2)}$$

where ν is the fluid viscosity, $\mathrm{d}\xi$ is the length of an infinitesimally small material line segment and γ is the turbulent rate of strain associated with material line deformation (Monin & Yaglom 1975). Assuming that γ is isotropic (an assumption that will be more closely examined later), the length of a material line segment is thus given by:

$$\mathrm{d}\xi(t) = \mathrm{d}\xi_0 \mathrm{e}^{\gamma t} \quad \text{(A2-3)}$$

provided that $\mathrm{d}\xi(t) < \eta$ for all t; a condition that can be met by making the initial segment length $\mathrm{d}\xi_0$ small enough. For a material line being traced out by a point source sinking at a speed w, the initial segment length is given by $\mathrm{d}\xi_0 = w\,\mathrm{d}t$, where $\mathrm{d}t$ is a small time step. The total length of the material line traced out by the falling particle is given by integrating over the path through time:

$$\xi(t) = \frac{w}{\gamma}(\mathrm{e}^{\gamma t} - 1) \quad \text{(A2-4)}$$

This gives the length of a material line traced out by a point moving in a uniform direction at speed w under isotropic turbulent straining.

Appendix 3. Variance of turbulent rate of strain

The rate of strain associated with the turbulent field $\gamma(\mathbf{x}, t)$ is not constant but fluctuates in time and space about a mean value $\bar{\gamma}$ with standard deviation σ that is of the order of $\bar{\gamma}$ (cf. Girimaji & Pope 1990). The length scale of these fluctuations is the Taylor micro-scale λ_T and the time scale is $T_T = \lambda_T/U \approx 4/\bar{\gamma}$ (e.g. Tennekes & Lumley 1972). For a small line segment drifting freely in the fluid, its relative rate of change is given by $\gamma(t)$ which gives:

$$\mathrm{d}\xi(t) = \mathrm{d}\xi_0 \mathrm{e}^{\int_0^t \gamma(t)\mathrm{d}t} \quad \text{(A3-1)}$$

analogous to Eq. (A2-3) for uniform straining. For $t > T_T$, the exponential factor tends to $\mathrm{e}^{\bar{\gamma}t}$ for all initial conditions. However, for $t < T_T$, the exponential factor can range from 1 (no net straining) to $\mathrm{e}^{2\bar{\gamma}t}$ (maximum net straining) depending on the time scale and initial conditions.

For a material line laid out by a sinking particle, the spatial coordinate z can be transformed to time by $z = wt$. Thus, for $t > \lambda_T/w$, there are significant spatial variations of stretching along the length of the material line.

Editorial responsibility: Otto Kinne (Editor), Oldendorf/Luhe, Germany

Submitted: January 14, 2004; Accepted: July 27, 2004
Proofs received from author(s): November 22, 2004